eman ta zabal zazu
Universidad del País Vasco
Euskal Herriko Unibertsitatea
ZIENTZIA ETA TEKNOLOGIA FAKULTATEA
FACULTAD DE CIENCIA Y TECNOLOGÍA

Trabajo Fin de Grado
Grado en Física

Global properties of charged black holes with cosmological constant

Autora:
Ángela Borchers Pascual

Director:
Raül Vera

Leioa, 18 de Julio de 2019

Abstract

In General Relativity, the causal structure of spherically symmetric spacetime solutions can be studied by the so-called Penrose diagrams. Based on conformal transformations, this technique is used to compactify spacetime manifolds, in order to make its causal relationships more evident. In this work, we review several solutions to Einstein's equation of gravity, constructing in each case the associated conformal diagram. Different black hole solutions are studied, together with the de Sitter spacetime, a vacuum solution that considers a positive cosmological constant. Eventually, we give an account of the global properties of charged black holes with positive cosmological constant.

Acknowledgements

En primer lugar, quiero agradecer a Raül por haberme dado la oportunidad de adentrarme en el campo de la relatividad general. Pero sobre todo por transmitirme su pasión por la física, por sus sugerencias y consejos, además del apoyo y toda la ayuda brindada durante este año.

A Sofía, Irene, Jokin, Asier, Elena, Mikel, Aritz... gracias por haber sido parte de estos años de tensión pero también de mucha alegría. Desde los paseos en el Arboretum, hasta las tardes de biblioteca en las que no faltaba el bocadillo de queso o nocilla...

To the people I met in Finland, kiitos much for your kind advices and special moments we shared. From that wonderful night at -20^{o} in northern Lapland, watching the northern lights dance in the sky, to that computer lab session on a Friday evening, which seemed to last forever. Se on erittäin ystävällistä sinulta!

Y dado que las últimas páginas fueron escritas desde Palma, gràcies también a la gente de la UIB: Cecilio, Toni, Rafel, Maite, Héctor, Rodrigo, y en especial a Sascha y Alicia, por tratarme tan bien y acogerme estos meses en vuestro grupo.

Finalmente, me toca dar las gracias a mi familia y amigos más cercanos, por estar ahí, por vuestro apoyo y confianza en mí.

Contents

Abstract **III**

1 Introduction **1**

2 Brief Review of General Relativity **3**
2.1 Causal Structure of Spacetime 5
2.2 Einsteins's Equation of Gravity 6
2.3 Static and Spherically Symmetric Solutions 7

3 Penrose-Carter Diagrams **8**
3.1 Conformal Compactification 8
3.2 Various "types" of Infinity? 10
3.3 Example: Minkowski Spacetime 10

4 The Schwarzschild Black Hole **13**
4.1 Kruskal-Szekeres 13
4.2 Penrose diagram 14

5 The Reissner-Nordström Black Hole **17**
5.1 Solution 17
5.2 Penrose diagram 20
5.2.1 Causality and Horizons 21
5.3 Collapse of a Charged Black Hole 22

6 De Sitter Universe **23**
6.1 De Sitter spacetime 23
6.2 The Schwarzschild - de Sitter solution 25

7 Charged Black Holes with Cosmological Constant **27**
7.1 The Reissner-Nordström-de Sitter solution 27

8 Conclusions **31**

References **V**

1 Introduction

The notion of causality is fundamental to every mathematical theory in physics. In General Relativity, Einstein's theory of gravity, the fabric of spacetime can have non-trivial geometries, and causal relations can become complex to study. The global causal structure of spacetime was first studied mainly by Roger Penrose (1972), Stephen Hawking and John Ellis (1973). In particular, Penrose introduced a technique based on conformal transformations, namely Penrose diagrams, that simplified in great measure the analysis of the global properties of spacetime [15], particularly those of the black hole solutions.

Black holes are vacuum solutions to Einstein's equation, which for a long time, were thought to be a mathematical solution that had no physical relevance. However, after the discovery of neutron stars in 1967 by Jocelyn Bell Burnell, gravitationally collapsing objects became a possible mechanism for the formation of black holes. Indeed, astrophysical stellar-mass objects are expected to collapse at the end of their life cycle an result in a stable black hole.

The only spherically symmetric solution to Einstein's equation for vacuum is the Schwarzschild metric, characterized by one parameter: the mass of the object generating the gravitational field, and which leads to the description of Schwarzschild black holes. Besides, according to the no-hair theorem, stationary, asymptotically flat black hole solutions are uniquely characterized by three externally observable parameters: mass, angular momentum and charge. Yet, astrophysical black holes appear to possess no charge and belong to the Kerr family, the set of uncharged rotating black holes (the Schwarzschild black hole is as a particular case of the Kerr family with zero angular momentum).

Therefore, focusing on charged black holes, which in principle are not found in our universe, might seem surprising for the reader. The main reason, beyond the curiosity for fundamental understanding we all share, is that the solution to Einstein's equation for such bodies gives rise to important features, which might be more difficult to understand in other types of spacetimes. The Kerr solution has no spherical symmetry, which makes the causal structure complex to study. However, the global structure of the Kerr and Reissner-Nordström (RN) solutions share some properties. The RN solution is, on the other hand, spherically symmetric, and the mathematical treatment becomes much more straightforward than in the former case. Therefore, understanding the peculiarities of the RN spacetime might probably be helpful for other solutions, which involve, for example, the presence of angular momentum.

Besides, the cosmological constant has attracted much attention lately. Since 1998 observational studies of type Ia supernovae have shown that the expansion of the universe is accelerating, apparently implying that the cosmological constant (Λ), which is associated to the vacuum energy, has a small but positive value. This term was originally introduced by Einstein in 1917, in order to balance the effect of gravity and to obtain a static universe, an idea that seemed to be accepted at that time.

Thus, the aim of this work is to give an account of the causal structure of the spacetime solution of a charged black hole with a positive cosmological constant. In the first chapters, we give a brief introduction to General Relativity, in addition to the main concepts of Penrose's conformal theory. The following sections are devoted to studying several solutions to Einstein's equation, including different black hole and de Sitter spacetime solutions. Besides, the associated Penrose diagram is built in each solution, and its main characteristics are explained. Eventually, the causal structure of charged black holes with a positive cosmological constant is studied.

2 Brief Review of General Relativity

The theory of General Relativity (GR), proposed by Albert Einstein a bit more than 100 years ago, is a theory of gravitation. Soon after the formulation of Special Relativity in 1905, Einstein began an obscure intellectual journey to find the precise mathematical expression for gravity. Newton's theory of gravitation was not consistent with Special Relativity, in particular, with the idea of instantaneous influence that one body could have from another. Instead of modifying his theory, a theory that already revolutionized our ingrained notions of space and time, Einstein followed an entirely new path.

The new theory, proposed in 1915, states that spacetime needs not be flat as in Special Relativity, it can be curved. This curvature, which can be described by a spacetime metric, is related to the matter content of the spacetime. Hence, freely falling bodies in a gravitational field will follow geodesics, extremal curves, of the curved spacetime and gravity will arise as a consequence of the curvature of the spacetime.

Besides, the theory has many predictions that have been well supported by observations and experiments. The gravitational redshift effect, existence of black holes, emission of gravitational waves, or the expansion of the universe are some of them. One of the first evidence of the theory was the correct prediction of the precession of the perihelium of Mercury, already proved by Einstein. Many tests have been done since then. Indeed, important observational confirmations have been made in the last few years. Gravitational waves were directly detected for the first time in 2015 [1], by the LIGO collaboration, and many more have been identified since then. In fact, five potential detections were made in the past month of April, during the O3 run of LIGO and Virgo detectors. Moreover, measurements made by ESO's Very Large Telescope revealed the effect of gravitational redshift around the massive black hole at the Galactic center of the Milky Way galaxy, in July 2018 [2]. Another recent evidence is the image of the supermassive black hole at the center of the galaxy M87 [3], a powerful confirmation of the existence of black holes and evidence of the "shadow" of such bodies.

The following sections provide a brief summary of the mathematical background of GR. Einstein's field equation is presented, as well as some characteristics of its solutions which will be carefully studied in future sections.

Manifolds and the Metric Tensor

The first task is to describe a manifold, one of the most fundamental notions in differential geometry. In the case of pre-relativity and Special Relativity physics, every event that takes place in the spacetime can be one-to-one mapped into $\mathbb{R}^4$. In the case of GR, however, a more general topological object is needed: a manifold. An n-dimensional manifold is a set that, locally, has the differential structure of $\mathbb{R}^n$, but might have different global properties. The spacetime in GR will be described by a 4-dimensional manifold.

This means one can consider different charts $\psi_\alpha, \psi_\beta ...$ that map a subset of the spacetime manifold $\mathcal{M}$ into a new subset of $\mathbb{R}^4$ (see Figure 1). Besides, one can perform a coordinate change between regions of $\mathbb{R}^4$ which are the image of the overlapped area of the subsets at the manifold (regions in turquoise blue).

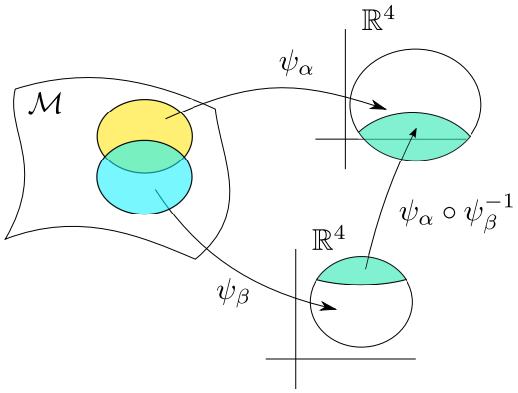

Figure 1: Diagram illustrating the mapping for two different charts.

Moreover, we are interested in Lorentzian manifolds, this is, the manifold is endowed with a metric $g_{\mu\nu}$ defined at every point, which locally determines the geometry of spacetime. The metric is a non-degenerate tensor (can be thought of as an invertible matrix) that determines lengths and angles between vectors. In particular, a vector X^μ at a point is said to be

$$\begin{aligned} \text{timelike} \quad & \text{if} \quad g_{\mu\nu}X^\mu X^\nu < 0 \\ \text{spacelike} \quad & \text{if} \quad g_{\mu\nu}X^\mu X^\nu > 0 \\ \text{null} \quad & \text{if} \quad g_{\mu\nu}X^\mu X^\nu = 0. \end{aligned} \tag{2.1}$$

When the vector is an infinitesimal variation we have

$$ds^2 = g_{\mu\nu}dx^\mu dx^\nu,$$

named as line element. Here, Einstein's summation notation has been introduced, this is, repeated superscripts and subscripts indices are summed over. Note also that it is natural to use the words "line element" and "metric" interchangeably.

At each point of the manifold we can define a basis of vectors that determine a vector space, called tangent space. In particular, a Lorentzian metric is such that for each point $p \in \mathcal{M}$ there exists a basis of vectors of the tangent space X_a^μ, with $a : 0, 1, 2, 3$, such that $g_{\mu\nu}X_0^\mu X_0^\nu < 0$ and $g_{\mu\nu}X_i^\mu X_i^\nu > 0$ for $i = 1, 2, 3$.

2.1 Causal Structure of Spacetime

In Special Relativity, the spacetime manifold is flat and is known as the Minkowski spacetime. In cartesian coordinates its metric is given by

$$ds^2 = -dt^2 + dx^2 + dy^2 + dz^2,$$

where the speed of light has been set to unity, $c = 1$. In spherical coordinates, this is, $x = r\sin\theta\cos\phi$, $y = r\sin\theta\cos\phi$, $z = r\cos\theta$, it can be rewritten as

$$ds^2 = -dt^2 + dr^2 + r^2(d\theta^2 + \sin^2\theta d\phi^2),$$

where $r > 0, 0 < \theta < \pi$ and $0 \leq \phi < 2\pi$. The causal structure of a particular event at a point in $\mathbb{R}^4$ is defined by its light cone, depicted in Figure 2.

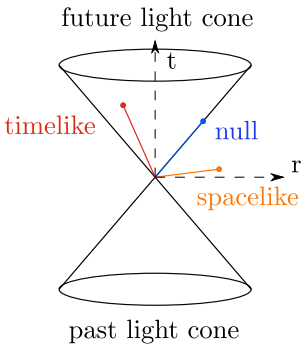

Figure 2: Causal structure of spacetime in special relativity embedded in a spacetime diagram.

The region outside the light cone is not accessible for any observer, not even for light. Only events lying inside the cone are reachable for particles with mass. Besides, light (and gravitational waves) follows null trajectories, determining the shape of the light cone (hence the name).

In the case of General Relativity, where the spacetime manifold is not necessarily flat, things become more complicated. Locally, the properties of the spacetime manifold are the same as in $\mathbb{R}^4$, and the structure of the light cones is the same as in Special Relativity. However, global properties can be significantly different. In the case of black hole solutions light cones appear to twist, singularities emerge, and causal horizons "divide" the spacetime into regions, which have particularly complicated causal relations. Hence, the goal is to portray the causal structure so that causal relationships become more clear.

Curvature

A *derivative operator* or *covariant operator*, ∇, on a manifold $\mathcal{M}$ endowed with metric $g_{\mu\nu}$, for a vector X^λ is

$$\nabla_\mu X^\lambda = \partial_\mu X^\lambda + \Gamma^\lambda_{\mu\nu} X^\nu \quad .$$

$\Gamma^\lambda_{\mu\nu}$ is called the *Christoffel symbol*, and is an essential object used to describe the curvature of a manifold. In differential geometry, vectors from different nearby tangent spaces have to be related in some specific way. The information about this particular "connection" between tangent spaces is contained in this symbol, which is constructed from the metric in the following way

$$\Gamma^\lambda_{\mu\nu} = \frac{1}{2} g^{\lambda\sigma}(\partial_\mu g_{\nu\sigma} + \partial_\mu g_{\sigma\mu} - \partial_\sigma g_{\mu\nu}).$$

On the other hand, it can be shown that the *geodesic equation* for a parameterized curve $x^\mu(\lambda)$ is

$$\frac{d^2 x^\mu}{d\lambda^2} + \Gamma^\mu_{\rho\sigma} \frac{dx^\rho}{d\lambda} \frac{dx^\sigma}{d\lambda} = 0.$$

The last and probably most important concept in this section is the *Riemann tensor*. All the information about the curvature of a manifold is encapsulated in this tensor, which is determined from the connection by

$$R^\rho_{\sigma\mu\nu} = \partial_\mu \Gamma^\rho_{\nu\sigma} - \partial_\nu \Gamma^\rho_{\mu\sigma} + \Gamma^\rho_{\mu\lambda}\Gamma^\lambda_{\nu\sigma} - \Gamma^\rho_{\nu\lambda}\Gamma^\lambda_{\mu\sigma}.$$

The Ricci tensor is the contraction of the first and third indices of the Riemman tensor, this is,

$$R_{\mu\nu} = R^\lambda_{\mu\lambda\nu}.$$

On the other hand, the trace of the Ricci tensor is the Ricci scalar,

$$R = R^\mu_\mu = g^{\mu\nu} R_{\mu\nu},$$

and finally, the Einstein tensor is defined by

$$G_{\mu\nu} = R_{\mu\nu} - \frac{1}{2} R g_{\mu\nu}.$$

2.2 Einsteins's Equation of Gravity

Einstein came up with the conclusion that the curvature of a spacetime manifold is related to the matter content on it. This way, geodesics could explain the motion that bodies, under the influence of a gravitational field, were following in nature. Thus, the metric has to be related to a mathematical object that describes the mass and energy (since they are interchangeable in relativity). This object is the energy-momentum tensor $T_{\mu\nu}$, and is related to the metric by

$$R_{\mu\nu} - \frac{1}{2} R g_{\mu\nu} + \Lambda g_{\mu\nu} = 8\pi G T_{\mu\nu}. \tag{2.2}$$

This is Einstein's field equation of general relativity. [1]

[1] Here, Λ is the cosmological constant and G Newton's constant of gravitation. Note also that $c = 1$.

2.3 Static and Spherically Symmetric Solutions

Most of the work written here is devoted to studying solutions of Einstein's equation, in particular those that describe the gravitational field of a spherically symmetric, static body.

A spacetime is said to be *stationary* if the spacetime admits a timelike Killing vector field ξ^α, which expresses a "time translation symmetry". Furthermore, a spacetime is *static* if it is stationary and if there exists a family of spacelike hypersurfaces Σ which are orthogonal to the orbits of the isometry [18]. Mathematically, this can be expressed as

$$\xi^\alpha = g\ \nabla^\alpha f.$$

Here, g and f are two functions, where $f = C \in \mathbb{R}$ determines for each C a spacelike hypersurface. This is the condition that a timelike Killing vector field needs to satisfy so that the spacetime is static.

A spacetime is said to be *spherically symmetric* when its isometry group contains a subgroup isomorphic to the SO(3) group [18]. The SO(3) isometries can be interpreted as rotations, and this implies that the metric of a spherically symmetric spacetime stays invariant under such rotations. Because of the SO(3) isometries, the spacetime metric induces a metric at each point, with a part proportional to the metric of a 2-sphere, $d\Omega^2 = d\theta^2 + \sin^2\theta d\phi^2$. Besides, it can be shown that in the case of a static spacetime, the factor of proportionality only depends on a spacelike coordinate r.

Eventually, the metric of any static spherically symmetric spacetime can be written as

$$ds^2 = g_{\mu\nu}(r)\ dx^\mu dx^\nu + \mathcal{R}^2(r) d\Omega^2,$$

so that $\mathcal{R}(r)$ determines the total area of the 2-sphere at r as $4\pi\mathcal{R}^2(r)$. Whenever $\nabla^\alpha\mathcal{R} \neq 0$ we can always choose r such that $\mathcal{R} = r$ and $t = C$, which leads to

$$ds^2 = -e^{\nu(r)}dt^2 + e^{\lambda(r)}dr^2 + r^2(d\theta^2 + \sin^2\theta d\phi^2). \tag{2.3}$$

Let us note that the Einstein equation for vacuum implies $\nabla^\alpha\mathcal{R} \neq 0$.

3 Penrose-Carter Diagrams

The study of the causal structure in a curved spacetime manifold can, in general, be extremely challenging. Even in the case of highly symmetric spacetimes, it is hard to visualize such structures. Part of the problem comes from the fact that we have to deal with infinite size spacetimes, being the spacetime itself a higher-dimensional geometric object.

Conformal diagrams (Penrose-Carter diagrams, or just Penrose diagrams) are two - dimensional spacetime diagrams with a particular feature: infinity is "squashed down" by introducing what is called a conformal transformation. A conformal transformation is essentially a local change of scale which preserves the causal structure of spacetime. In other words, light cones are left invariant. A conformal transformation is given by

$$\tilde{g}_{\mu\nu}(x) = \Xi^2(x) g_{\mu\nu}(x), \tag{3.1}$$

where $\Xi(x)$ is a smooth non-vanishing function and $\tilde{g}_{\mu\nu}$ the conformally-related metric. These transformations are basically a change of the geometry, so in the same way we can write

$$\widetilde{ds}^2 = \Xi^2(x) ds^2. \tag{3.2}$$

The invariance of light cones under such transformations can be then easily proved. Consider a vector X^μ on a manifold $\mathcal{M}$ endowed with metric $g_{\mu\nu}$. Since $\Xi^2(x) > 0$, then

$$\begin{aligned} g_{\mu\nu}X^\mu X^\nu < 0 &\iff \tilde{g}_{\mu\nu}X^\mu X^\nu < 0 \\ g_{\mu\nu}X^\mu X^\nu > 0 &\iff \tilde{g}_{\mu\nu}X^\mu X^\nu > 0 \\ g_{\mu\nu}X^\mu X^\nu = 0 &\iff \tilde{g}_{\mu\nu}X^\mu X^\nu = 0. \end{aligned}$$

Hence, timelike/null/spacelike trajectories with respect to $g_{\mu\nu}$ will have the same character with respect to $\tilde{g}_{\mu\nu}$. In particular, null curves are left invariant and will always be portrayed at 45^o on conformal diagrams. (Here, the angle depends on the selected units or the inclination of the axes). Locally, the two metrics in (3.1) are said to be conformally equivalent.

3.1 Conformal Compactification

In short, a conformal diagram is a spacetime diagram characterized by a clever coordinate change, which converts an infinite space to a finite size. Thus, having infinity just a finite value away makes the causal structure much more evident. It is important to note that boundaries, which represent infinity, are not part of the original spacetime, and they are referred to as *conformal infinity*. The union of the original spacetime with conformal infinity is the so-called *conformal compactification*, which is a manifold with boundary [5].

The idea of this "shrinking" might be better visualized with the help of the following two examples.

First, let us imagine what the compactification process would look like in one dimension. The key here is to remember that the tangent function goes to infinity at $\pm\pi/2$. If one considers the inverse function infinities can be brought to a finite distance, and thus, the whole of $\mathbb{R}$ can be represented by a finite one-dimensional interval: $\mathbb{R} \to (-\pi/2, \pi/2)$. Here, $\pi/2$ and $-\pi/2$ are not part of the interval, in the same way infinities are not part of $\mathbb{R}$. Note that in this case we have two "objects" representing infinity.

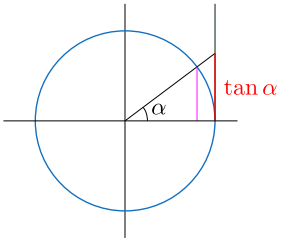

Figure 3: Value of the tangent function in a unit circle.

The second example is the stereographic projection, a mapping that projects a sphere into a two-dimensional plane.

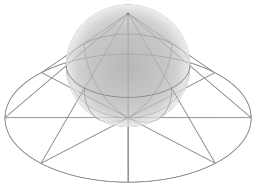

Figure 4: Stereographic projection. Figure from Wikipedia.

Let us imagine we want to project every point of the surface of a sphere, down to a plane tangent to the south pole, by taking the north pole as a reference. We start projecting the south pole, continue to the east, west and so on, until we arrive at the north pole. How do we project the north pole itself? Right, it goes to infinity.

So infinity is being represented by a single point. It is worthwhile to spend some time thinking on this. It is highly relevant for Penrose diagrams since infinity will also be represented by points. Now, the result of the projection is an infinite plane, which represents $\mathbb{R}^2$. It should be noted again that infinity is not a real number, is not part of $\mathbb{R}^2$. So according to the projection-process just made, given the set of points of the surface of a sphere and taking the top point out, we get $\mathbb{R}^2$. Or the other way round. Given $\mathbb{R}^2$ and infinity, we get a 2-sphere. Hence, infinite space is squashed down to a finite size, the sphere. This is how the compactification process of a Penrose diagram looks like in essence.

Nevertheless, it might be confusing for the reader to learn about this apparently "simple" example. It will be, however, a handy tool for visualizing conformal diagrams. The present case is a two-dimensional geometric object while conformal maps consider, in general, higher dimensional geometries. We will, therefore, come back to it in future chapters.

3.2 Various "types" of Infinity?

In 1964, the English mathematician and physicist Roger Penrose developed his theory about the conformal structure of spacetime. All along his work he refers to different kinds of infinities, which are convenient to mention since they are one of the most fundamental elements of conformal diagrams. The following list provides a convenient description of each of them [13], for a static and spherically symmetric spacetime with metric (2.3).

$i^+ \equiv$ future timelike infinity: the region $t \to +\infty$ at finite radius r

$i^- \equiv$ past timelike infinity: the region $t \to -\infty$ at finite radius r

$i^0 \equiv$ spacelike infinity: the region $r \to \infty$ at finite time t

$\mathscr{I}^+ \equiv$ future null infinity: the region $t + r \to +\infty$ at finite $t - r$

$\mathscr{I}^- \equiv$ past null infinity: the region $t - r \to -\infty$ at finite $t + r$

($\mathscr{I}$ is a script I, and $\mathscr{I}^\pm$ is pronounced as "scri-plus" or "scri-minus"). As we shall see, i^+, i^-, i^0 are represented by dots, even if they are originally regions (recall the 2-sphere example). On the other hand, $\mathscr{I}^-$ and $\mathscr{I}^+$ represent the segments where all null geodesics begin and end, respectively.

3.3 Example: Minkowski Spacetime

Minkowski spacetime is the simplest vacuum solution in GR. Its metric is the so-called Lorentz metric η, and as it was mentioned before, it is the mathematical background of the theory of Special Relativity. We recall that in spherical coordinates the metric reads

$$ds^2 = -dt^2 + dr^2 + r^2 d\Omega^2,$$

where $d\Omega^2 = d\theta^2 + \sin^2\theta d\phi^2$. The coordinate ranges are $-\infty < t < \infty$, $0 < r < \infty$, $0 < \theta < \pi$ and $0 \leq \phi < 2\pi$. Note that $r = 0$ is not included in spherical coordinates. In order to build the corresponding Penrose diagram, the first step is to switch to null radial coordinates

$$u = t - r, \qquad v = t + r, \tag{3.3}$$

with ranges $-\infty < u < \infty$, $-\infty < v < \infty$ and $v > u$. The Minkowski metric is now

$$ds^2 = -dudv + \frac{1}{4}(v-u)^2 d\Omega^2. \tag{3.4}$$

Once null coordinates have been considered, Penrose's technique comes into play. New null coordinates are defined in a way such that the infinities of u, v are converted into finite values. A smart idea is to use the tangent function (just as in the example mentioned above), so that

$$\tan U = u, \qquad \tan V = v, \tag{3.5}$$

transform the metric the following way

$$ds^2 = \sec^2 U \sec^2 V \left(-dUdV + \frac{1}{4}\sin^2(V-U) d\Omega^2 \right). \tag{3.6}$$

Thus, the coordinates' ranges are no longer reaching infinity: $-\pi/2 < U < \pi/2$, $-\pi/2 < V < \pi/2$, with $V > U$. On the other hand, note that the metric (3.6) is conformal to the metric $\tilde{g}$ given by

$$\widetilde{ds}^2 = -4dUdV + \sin^2(V-U)d\Omega^2, \tag{3.7}$$

with the conformal factor $\Xi^2(U,V) = \frac{1}{4}\sec^2 U \sec^2 V$. In order to get a more usual form of the metric a last coordinate change is made. The new coordinates are written in terms of the advanced and retarded null coordinates, $T = V + U$, $R = V - U$, with ranges

$$-\pi < T + R < \pi, \quad -\pi < T - R < \pi, \quad R > 0. \tag{3.8}$$

The metric is now

$$ds^2 = \Xi^2(T,R)\left[-dT^2 + dR^2 + \sin^2 R d\Omega^2\right], \tag{3.9}$$

where the conformal factor is given by

$$\Xi^2(T,R) = \frac{1}{4}\sec^2[(T+R)/2]\sec^2[(T-R)/2].$$

So far, a confomal compactification has been performed, transforming the coordinate ranges into finite values. Therefore at this point, the conformal diagram can already be constructed, by representing the coordinate ranges of $\{T, R\}$ given by (3.8). As illustrated in Figure 5 the left side of the triangle is not part of conformal infinity.

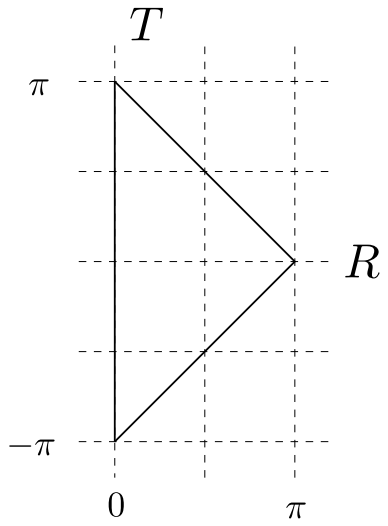

Figure 5: Diagram illustrating the region conformal to Minkowski space.

Minkowski space is represented by the interior of the above diagram. Infinities are not part of the original spacetime. In fact, the conformal diagram subdivides the boundaries, the so-called conformal infinity, into five different "regions": $i^{\pm}, i^0$ and $\mathscr{I}^{\pm}$ (see Figure 6). Note that the infinities (i^+, i^-, i^0) are represented at the diagram by dots, just like in the stereographic projection example mentioned above.

Another important thing to mention is that, since two angular coordinates have been omitted, every point of the conformal diagram actually represents a 2-sphere. Hence, i^0 represents a sphere of infinite radius, while if we move towards the origin the size of the sphere will decrease, until $r = 0$, which is a point (a line in $\mathbb{R}^4$).

Interestingly, both future and past infinities have a different mathematical structure than the rest of points of the conformal region. Recalling once again the two-dimensional example in section 3.1, just like the north pole does not represent a point of $\mathbb{R}^2$, i^+ and i^- do not represent a 2-sphere. Clearly, there has to be a deeper mathematical description for them.

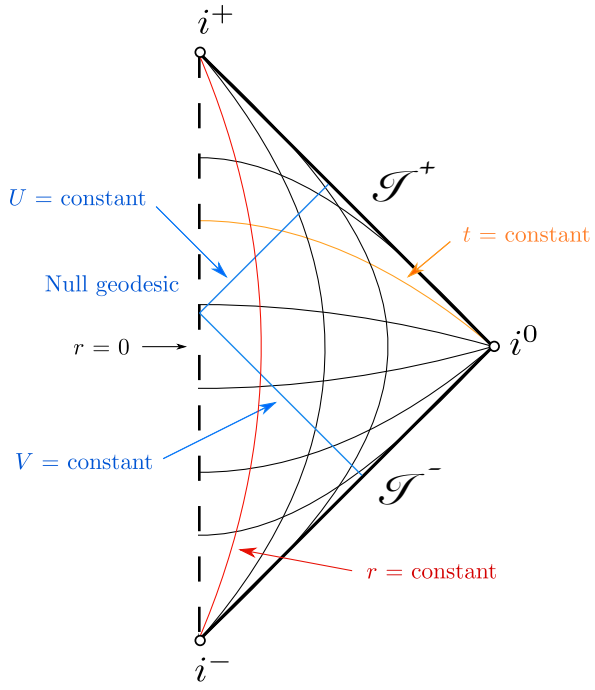

Figure 6: Penrose diagram for Minkowski spacetime.

Since the metric (3.9) in terms of $\{T, R\}$ is conformal to the one in terms of $\{t, r\}$, constant r and t trajectories can be illustrated in the above diagram.

In fact, timelike geodesics, trajectories followed by freely falling observers, all start and end at i^- and i^+ respectively. On the other hand, since null trajectories are left invariant under conformal transformations, all null geodesics begin and end at $\mathscr{I}^-$ and $\mathscr{I}^+$ respectively, represented by straight lines at $\pm 45^o$. Similarly, spacelike geodesics both begin and end at i^0.

Nevertheless, the structure of the Penrose diagram for Minkowski spacetime is rather "unuseful" in this case. It does not bring new information. Conformal diagrams are indeed much more helpful when the studied spacetime has higher complexity. In the next sections, different kinds of black hole solutions are studied, which are more complex than the present case, and thus, Penrose diagrams will become a crucial tool to understand the global properties of such spacetimes.

4 The Schwarzschild Black Hole

The description for the gravitational effect created by a spherically symmetric body was found by Karl Schwarzschild in 1916, months after Einstein had published his field equation. This solution is indeed of great interest in astrophysics, since it describes to a good approximation the exterior gravitational field of celestial objects, such as the Sun, the Earth or black holes.

4.1 Kruskal-Szekeres

The spherically symmetric solution of Einstein's equation for vacuum[2]

$$R_{\mu\nu} = 0,$$

outside a spherically symmetric body is

$$ds^2 = \frac{32m^3}{r}\, e^{-r/2m}(-d\tau^2 + dX^2) + r^2 d\Omega^2, \tag{4.1}$$

where $r(\tau, X) > 0$ is given implicitly by

$$X^2 - \tau^2 = -\left(1 - \frac{r}{2m}\right) e^{r/2m}. \tag{4.2}$$

This is known as the Schwarzschild-Kruskal metric, which is written in terms of the coordinates (τ, X, θ, ϕ), the so-called Kruskal-Szekeres coordinates. Here, m is interpreted as the gravitational mass of the body [3]. Besides, there is a physical singularity at $r = 0$, since some relevant curvature scalars, such as $R_{\rho\sigma\mu\nu}R^{\rho\sigma\mu\nu}$, tend to infinity there.

Since $r > 0$, equation (4.2) yields

$$X^2 - \tau^2 > -1. \tag{4.3}$$

Note this is the only restriction for the coordinate ranges. Therefore, the spacetime diagram can be drawn in the following way.

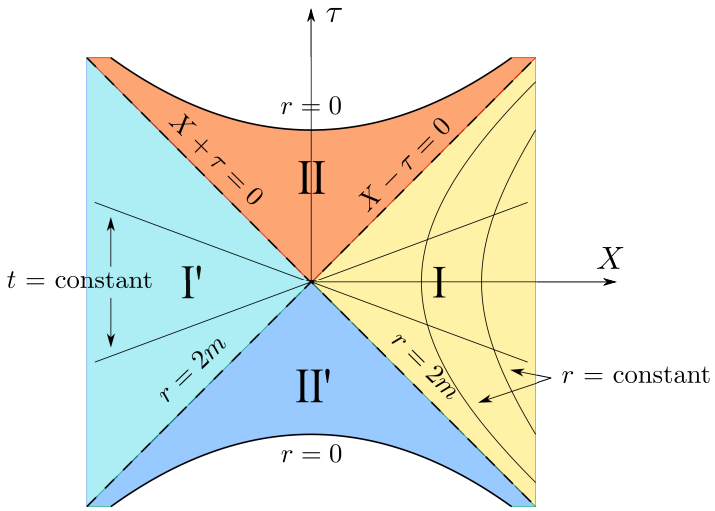

Figure 7: The Kruskal spacetime.

[2] In this case, the energy-momentum tensor is $T_{\mu\nu} = 0$, since we are interested in exterior solutions.
[3] Here, the following constant is set to unity: $8\pi G = 1$, so that mass and lenght have the same magnitude.

Here, the coloured regions, regions I, I', II and II', all satisfy (4.3). On the other hand, there are two diagonal lines at $r = 2m$, which according to (4.2) correspond to $X \pm \tau = 0$. Besides, null geodesics, which are given by $X \pm \tau =$ constant, are portrayed at $\pm 45^{\rm o}$.

Now, in region I, one can define a coordinate t by

$$\frac{t}{2m} = \ln\left(\frac{X+\tau}{X-\tau}\right) = 2\tanh^{-1}(\tau/X). \tag{4.4}$$

Using equations (4.2) and (4.4), which give the relation between $\{\tau, X\}$ and $\{t, r\}$, the metric in (4.1) transforms into

$$ds^2 = -\left(1-\frac{2m}{r}\right)dt^2 + \left(1-\frac{2m}{r}\right)^{-1} dr^2 + r^2 d\Omega^2,$$

the so-called Schwarzschild metric. Region I corresponds precisely to the Schwarzschild spacetime, and this is the reason why Figure 7 is actually called the Kruskal *extension* of the Schwarzschild spacetime.

4.2 Penrose diagram

The coordinates of the Schwarzschild-Kruskal metric (4.1) have ranges: $-\infty < \tau < \infty$ and $-\infty < X < \infty$, with $X^2 - \tau^2 > -1$. The spacetime is infinite in size and thus, in order to built a Penrose diagram a conformal compacification of the spacetime needs to be performed. In the same way as in Minkowski spacetime, first, null coordinates are defined by

$$u = \tau - X, \qquad v = \tau + X,$$

with ranges $-\infty < u < \infty$, $-\infty < v < \infty$ and $uv < 1$. The metric (4.1) transforms then into

$$ds^2 = \frac{32m^3}{r}\, e^{-r/2m}\, du\, dv + r^2 d\Omega^2, \tag{4.5}$$

where $r(u, v)$ is given by

$$uv = \left(1-\frac{r}{2m}\right) e^{r/2m}\ . \tag{4.6}$$

Now the compactification process is carried out by considering new coordinates $\{U, V\}$ such that

$$\tan U = u, \qquad \tan V = v.$$

The coordinate ranges are now $-\pi/2 < U < \pi/2, -\pi/2 < V < \pi/2$ and $-\pi/2 < U+V < \pi/2$. The last step is to define timelike and spacelike coordinates:

$$T = U + V, \qquad R = U - V,$$

which have the following ranges: $-\pi < T + R < \pi, -\pi < T - R < \pi$, with $-\pi/2 < T < \pi/2$. The region conformal to the Kruskal extension is depicted in the following figure.

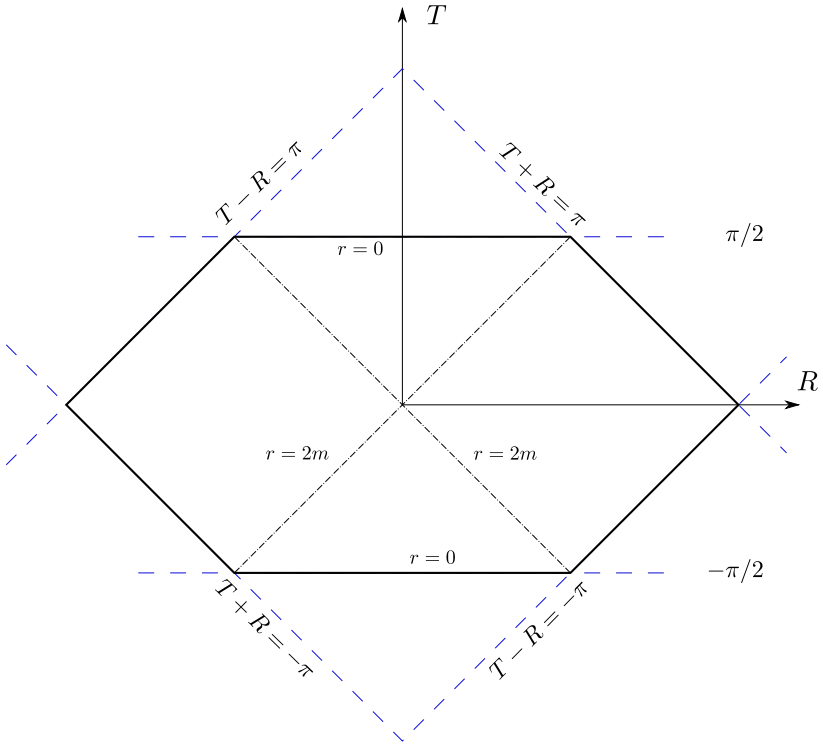

Figure 8: Conformal region of the Kruskal extension.

The Penrose diagram for the Kruskal extension of the Schwarzschild spacetime is therefore the following.

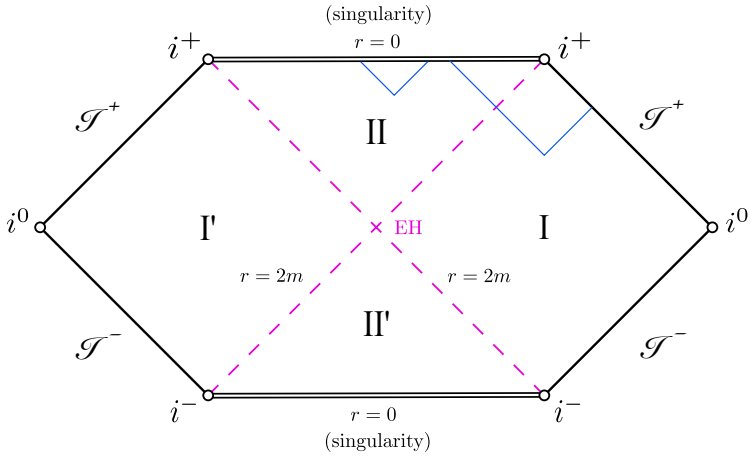

Figure 9: Penrose diagram for the Kruskal extension of the Schwarzschild black hole.

The extended Schwarzschild solution has four regions. In fact, it might be surprising to find more than one (same type of) infinity at the diagram. The region $2m < r < \infty$ are actually two regions, I and I'. Regions II and II', which span the region $0 < r < 2m$, are symmetric as well. However, I (I') and II (II') are fundamentally different. As mentioned, the Schwarzschild spacetime corresponds to region I, and it represents an asymptotically flat spacetime. This is, a spacetime for which, as $r \to \infty$, i^0 and $\mathscr{I}^{\pm}$ have the same structure as in the Minkowski space, named as asymptotic end (see Figure 10).

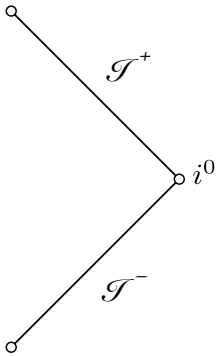

Figure 10: Asymptotic end structure of an asymptotically flat spacetime. The Kruskal spacetime has indeed two asymptotically flat end structures.

On the other hand, the lower region II' is referred to as *white hole*, while the upper region is named *black hole*. The $r = 2m$ null hypersurface dividing region I from II is known as a event horizon (EH).

Note again that null geodesics are portrayed at 45°. Besides, the singularity (at $r = 0$), which is represented by double lines, has a spacelike character. Therefore, any timelike trajectory entering region II will fall into the singularity with no way of avoiding it. Such trajectories will never reach $\mathscr{I}^+$ and will always stay in region II. Precisely, we define a black hole as the set of points whose causal curves do not arrive at $\mathscr{I}^+$, and for this reason, region II is referred to as a black hole.

Another thing that is important to understand is that the singularity at $r = 0$ is not "connected" to neither i^+ nor i^-, they are distinct. Indeed, Penrose diagrams might sometimes be a bit misleading. The fact that they both represent a boundary does not mean they are related. If one stays in region I, outside the event horizon, one will tend towards i^+ without hitting the singularity. Inside the EH, however, the only possible trajectory is the one that gets closer and finally arrives at the singularity, at a finite time. This can be better visualized in Figure 9.

Historically, the Kruskal-Szekeres (K-S) coordinates were proposed after the Eddington-Finkelstein (E-F) coordinates were introduced, and at the same time, these were defined from spherical coordinates (after the Schwarzschild metric). The reason for the number of regions in the Kruskal extension is the election of the E-F coordinates, which, in the Kruskal extension, lead to the description of four different regions of the spacetime.

There are some deep geometrical ideas that lie under these coordinate changes, which were explained at the beginning of section 2. As it was mentioned, there can be different coordinate changes between subsets of $\mathbb{R}^4$. The fundamental question one should ask then is, whether there exists any chart that covers a maximal range of the manifold. The answer in this case is yes, and this chart is, in fact, the Kruskal-Szekeres coordinate system.

5 The Reissner-Nordström Black Hole

A Reissner-Nordström black hole has mass and charge, but does not have angular momentum. The solution to Einstein's equation for such bodies was found independently by Reissner (1916) and Nordström (1918). Despite the fact that objects in our universe appear to be electrically neutral (a charged object would attract other matter with opposite charge), the causal structure of the RN spacetime is of great interest and is still a current research topic.

5.1 Solution

The Schwarzschild solution describes the geometry of a vacuum spacetime outside a spherically symmetric body. In the case of a charged body, there exists a source of energy-momentum due the charge of the object. The Einstein-Maxwell field equations for the description of a non-rotating charged spherical object are

$$R_{\mu\nu} - \frac{1}{2}Rg_{\mu\nu} = 2\left(F_{\mu\lambda}F^{\lambda}_{\ \nu} - \frac{1}{4}g_{\mu\nu}F_{\rho\sigma}F^{\rho\sigma}\right), \tag{5.1}$$

$$\nabla_\mu F^{\mu\nu} = 0, \tag{5.2}$$

where $F^{\mu\nu}$ is the electromagnetic strength field tensor. The spherically symmetric and bounded solution of equation (5.2) is

$$F_{\mu\nu} = \begin{pmatrix} 0 & e/r^2 & 0 & 0 \\ -e/r^2 & 0 & 0 & 0 \\ 0 & 0 & 0 & 0 \\ 0 & 0 & 0 & 0 \end{pmatrix}, \tag{5.3}$$

where the non-existence of magnetic monopoles has been assumed[4]. Here, e is the total electric charge of the body.

On the other hand, equation (5.1) with $F_{\mu\nu}$ given by (5.3), has a spherically symmetric asymptotically flat solution, known as the Reissner-Nordström metric,

$$ds^2 = -\Delta dt^2 + \Delta^{-1}dr^2 + r^2 d\Omega^2, \tag{5.4}$$

where

$$\Delta(r) = \left(1 - \frac{2m}{r} + \frac{e^2}{r^2}\right).$$

The function Δ has the following characteristics:
- If $e^2 > m^2$, the solution has a physical singularity at $r = 0$ ($R_{\rho\sigma\mu\nu}R^{\rho\sigma\mu\nu}$ blows up there).
- If $e^2 < m^2$, apart from the singularity at $r = 0$, the function Δ has two zeros at

$$r_\pm = m \pm \sqrt{m^2 - e^2},$$

and one if $e^2 = m^2$. In this work only the $e^2 < m^2$ case is studied. It includes the $e = 0$ case, and can therefore be seen as a generalization of the Schwarzschild black hole.

[4]From now on we consider $4\pi\epsilon_0 = 1$.

As mentioned, when $e^2 < m^2$ the function Δ has two zeros that "divide" the spacetime into three regions defined as

- Region I: $r_+ < r < \infty$
- Region II: $r_- < r < r_+$
- Region III: $0 < r < r_-$.

Now, we need to find a way of covering a maximal range of the spacetime manifold. In the case of the Schwarzschild solution we had a *single map*, which was the Kruskal-Szekeres coordinate system. We had two different regions depending on the covered range of the function r: region I/I' ($0 < r < 2m$) and II/II' ($2m < r < \infty$), and these were related by a *single pair* of coordinates: $\{\tau, X\}$.

A charged black hole has, however, regions I, II and III. In this case, *two pairs* of Kruskal-Szekeres coordinates have to be defined: one pair for regions I and II, and another for regions II and III. This is, we need *two charts*. The conformal diagram will then be constructed by "piecing" these two patches that lead to the mapping of a maximal range of the manifold.

Kruskal-Szekeres

On the one hand, it can be shown that for regions I and II the solution is given by [17],

$$ds^2 = -\frac{r_+ r_-}{r^2}\frac{e^{-2\kappa_+ r}}{\kappa_+^2}\left(\frac{r_-}{r-r_-}\right)^{\left(\frac{\kappa_+}{\kappa_-}-1\right)} du^+ dv^+ + r^2 d\Omega^2, \tag{5.5}$$

where the relation between the radial function $r(u^+, v^+)$ and the K-S coordinates $\{u^+, v^+\}$ is given implicitly by

$$u^+ v^+ = -e^{2\kappa_+ r}\left(\frac{r-r_+}{r_+}\right)\left(\frac{r-r_-}{r_-}\right)^{\kappa_+/\kappa_-}, \tag{5.6}$$

and

$$\kappa_\pm = \frac{(r_\pm - r_\mp)}{2r_\pm^2} \quad .$$

Note the similarity to equations (4.5) and (4.6), which were written in terms of the Kruskal coordinates of the Schwarzschild spacetime $\{u, v\}$.

Regions I and II are analogous to the ones in the Schwarzschild black hole, except that the diagonal lines "dividing" each region are now at $r = r_+$ instead of $r = 2m$. Constant r hypersurfaces are oppositely drawn in the two regions as well. In region II, r-constant hypersurfaces are spacelike while in region I they are timelike. Therefore, once at $r = r_+$, one can only get closer to the singularity of the black hole (until $r = r_-$) and cannot go back to region I.

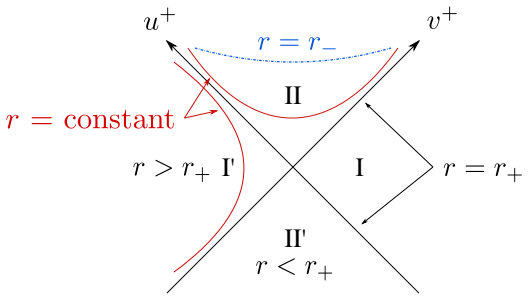

Figure 11: Coordinates u^+ and v^+.

The reason why these coordinates only cover two of the three regions is due the fact that coordinates $\{u^+, v^+\}$ do not behave well at $r = r_-$. Hence, new coordinates are considered $\{u^-, v^-\}$ in order to cover regions II and III, in which the metric reads [17]

$$ds^2 = -\frac{r_+ r_-}{r^2}\frac{e^{-2\kappa_- r}}{\kappa_-^2}\left(\frac{r_+}{r_+ - r}\right)^{\left(\frac{\kappa_-}{\kappa_+}-1\right)} du^- dv^- + r^2 d\Omega^2, \tag{5.7}$$

where

$$u^- v^- = -e^{-2\kappa_- r}\left(\frac{r_- - r}{r_-}\right)\left(\frac{r_+ - r}{r_+}\right)^{\kappa_+/\kappa_-}. \tag{5.8}$$

In region III, constant r surfaces have the same character as in region I, they are timelike. Note $r = 0$ is now at the boundary of the coordinate range. Since $\forall r : \; r < r_-$, r-constant trajectories are timelike, $r = 0$ is also timelike, and is referred to as naked singularity. Even though the Riemann tensor blows up there, $r = 0$ can be drawn in figure 12, since equation (5.8) is analytic there: $u^- = -1/v^-$. Hence, observers at region III who follow timelike trajectories can, in principle, avoid hitting the singularity[5]. Note also that coordinates u^- and v^- do not behave well at $r = r_+$.

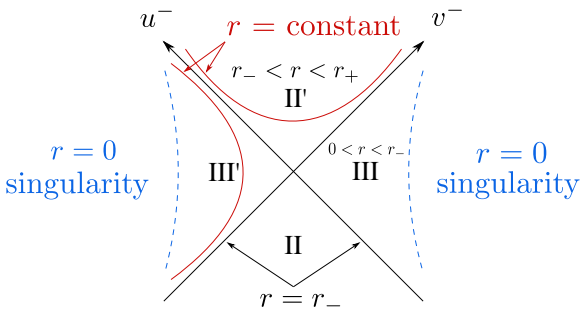

Figure 12: Coordinates u^- and v^-.

The spacetime manifold is therefore represented by *two charts* of "coordinate neighbourhoods" [10], $\{u^+, v^+\}$ for $r \neq r_-$, and $\{u^-, v^-\}$ for $r \neq r_+$. Precisely, the same way as the 2-sphere S^2 cannot be mapped into $\mathbb{R}^2$ by a single patch (recall, once again, the example mentioned in section 3.1). Two charts are needed to cover the 2-sphere, one for each pole. Thus, in order to cover the whole of the spacetime we consider two patches which, in the present case, overlap in region II. In this "piecing" process, both the $r = r_-$ hypersurfaces of the $\{u^+, v^+\}$ coordinate chart and the $r = r_+$ curves of the $\{u^-, v^-\}$ chart become null

[5] As we shall see in following sections, the appearance of instabilities at $r = r_-$ might change the structure of spacetime and thus, the character of the singularity.

(see Figures 11 and 12). With these ideas the conformal diagram of the Reissner-Nordström spacetime can be then constructed.

5.2 Penrose diagram

The conformal diagram of the maximally extended Reissner-Nordström solution is shown in Figure 13. The coordinate compactification process that needs to be followed is not explicitly given here, since it is analogous to the one performed for Minkowski and Schwarzschild spacetimes. Besides, it will be explicitly given (and extended) in the last section, in the study of the Reissner-Nordström black hole with cosmological constant.

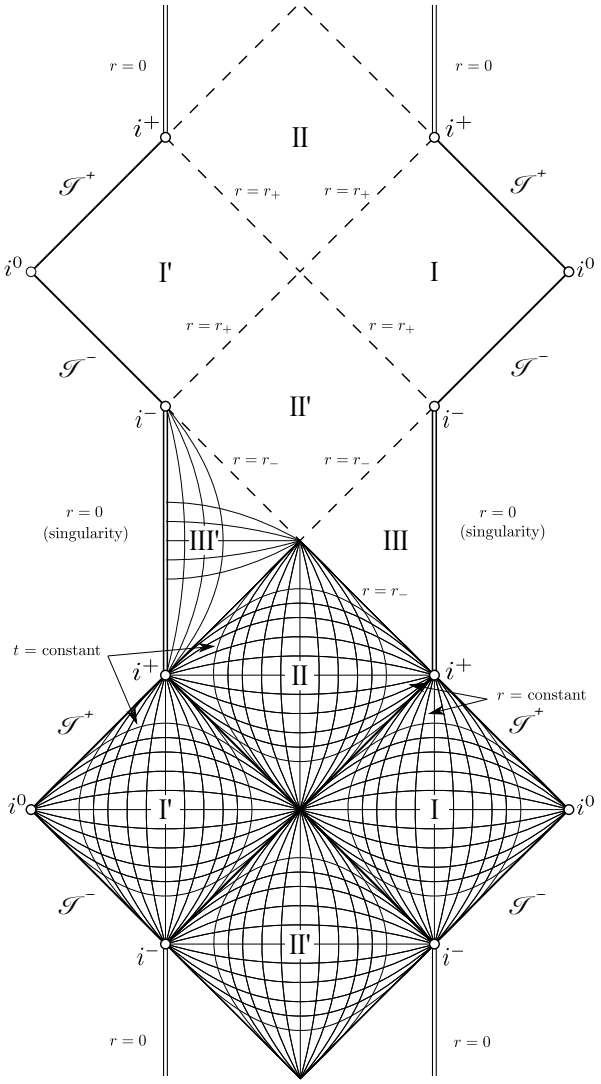

Figure 13: Penrose diagram for the Reissner-Nordström solution.

Note that an observer traveling from region II to III, getting closer to the singularity, could reemerge into region II', getting away from the black hole. However, region II' is at the same time connected to region I, a new asymptotically flat region. So, according to the diagram, one could travel from one universe to another, just by getting close enough to the singularity of the charged black hole.

If the above diagram is carefully studied, one might realise that the structure of future and past infinities, i^+ and i^-, is different from the rest of points of the spacetime, just as in the Minkowski space. Since curves with different radial values end up at i^+ and i^-, these do not represent a 2-sphere of a specific size. In fact, one can realize that these curves have all kind of values: $0 < r < \infty$. Therefore, i^+ and i^- actually represent regions and are in fact spheres of infinite radius that cover all the space.

5.2.1 Causality and Horizons

The causal structure is much more evident in a conformal diagram. In fact, one can recognize two types of horizons: an outer one lying on $r = r_+$ and an inner one at $r = r_-$. The former is an event horizon; this is, events happening inside such surface will never reach the part of $\mathscr{I}^+$ which could be attained by a spacelike geodesic from its position. Causal information will travel following timelike or null curves, which, as it can be seen in the diagram, will never pass through region I. Instead, they will either hit the singularity or reemerge into a new asymptotically flat region[6].

On the other hand, there is a Cauchy horizon at $r = r_-$, a boundary of the domain of validity of an initial value problem. Cauchy surfaces, spacelike or null surfaces, predict the evolution given an initial data set, and they intersect every timelike curve once and once only [9]. Having a Cauchy horizon implies the existence of a region (in this case $r < r_-$) where the evolution of the initial data cannot be predicted. Thus, predictability appears to break down at the inner horizon, which could be seen as a failure of determinism of the theory of General Relativity. Roger Penrose asserted this problem by proposing the strong cosmic censorship conjecture, which states that the maximal Cauchy development (the region of spacetime that can be predicted from initial data), is never part of a larger spacetime that could not be predicted. In the Reissner-Nordström solution, however, the spacetime can be extended beyond the Cauchy horizon, in apparent contradiction with the strong cosmic censorship. The missing piece of the puzzle is that instabilities appear to occur at such Cauchy horizon, as it will be explained in the next section.

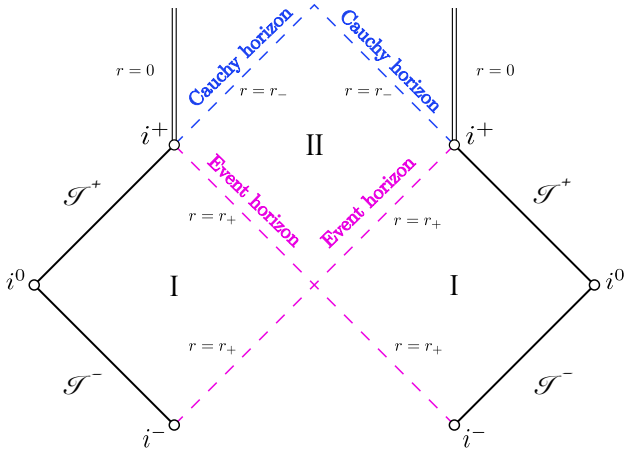

Figure 14: Event and Cauchy horizons in the Reissner-Nordström Penrose diagram.

[6] As it was said before, instabilities at the inner horizon might probably change the structure of the spacetime, transforming it into a spacetime structure similar to the Schwarzschild black hole solution. Thus, the only probable trajectory the information would follow would be the one hitting the singularity.

Instabilities at the Cauchy Horizon

Since light travels at $\pm 45^{o}$, an observer who is traveling through $r = r_{-}$ looking back in time, would see the entire future history of the universe at a finite time. Besides, one would watch the entire universe, since light from (the spatial) infinity, is reaching such horizon. Hence, any light wave traveling towards the Cauchy horizon would be infinitely blue-shifted, since an infinite number of events would be seen in a finite time. Thus, an observer traveling at such distance would see a bright white flash.

Besides, it has been argued that the Cauchy horizon is unstable [7], [16]. Linear perturbations become singular at the inner horizon, resulting in a spacetime that does not exhibit a Cauchy horizon, but a true singularity, similar to the Schwarzschild black hole case. The reason is that oscillations in the gravitational and electromagnetic field with finite frequency, are "observed" as infinite frequency waves at $r = r_{-}$ due to the fact that signals are infinitely blue-shifted. Nevertheless, these ideas are still under current investigation, since a proper mathematical demonstration of the instability of Reissner-Nordström has not been found yet.

5.3 Collapse of a Charged Black Hole

So far we have studied Einstein's equation for a spherically symmetric charged body in vacuum space. This is, the structure of the whole of the spacetime has been shaped as if the black hole had existed ever since the "beginning". A more realistic case is the study of a collapsing star that transforms into a black hole. Besides, it can also be described by a Penrose diagram. In fact, by the combination of two of them. First, the already known diagram is considered as a background universe, and second, the shrinking of a star is described by an independent conformal diagram. The superposition of the two of them describes this process, which can be seen in the following figure [18].

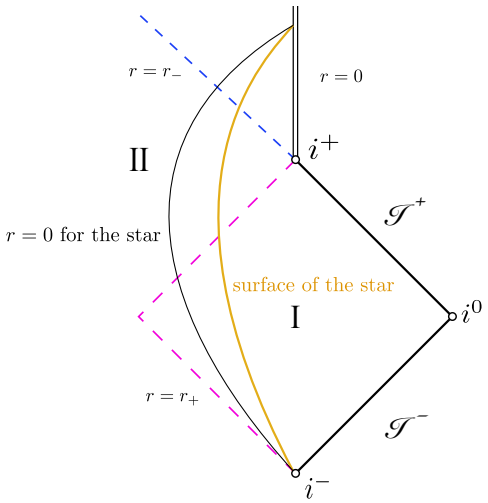

Figure 15: Penrose diagram of a collapinsg charged black hole.

6 De Sitter Universe

The spacetime solutions described so far are all asymptotically flat. At large distances they all approached the Minkowski spacetime structure, the so-called asymptotic end. Physically it can be thought of as all the fields going to zero as we travel far away from the sources. However, these solutions might not describe well what we observe in our universe. The cosmological constant (Λ), which is associated to the vacuum energy, appears to have a positive value. The solution to Einstein's equation for vacuum with positive cosmological constant was found by the Dutch astronomer Willem de Sitter in 1917. The solution is named after him as the de Sitter spacetime or de Sitter universe, since it is also used in the field of cosmology as a cosmological solution.

6.1 De Sitter spacetime

The *de Sitter* spacetime is the space with positive Ricci scalar, and has a topology $R^1 \times S^3$. Its metric can be written in terms of the spherical coordinates (t, χ, θ, ϕ),

$$ds^2 = -dt^2 + \alpha^2 \cosh^2(t/\alpha) \left[d\chi^2 + \sin^2 \chi (d\theta^2 + \sin^2 \theta d\phi^2) \right]. \tag{6.1}$$

Here, the coordinates have the following ranges: $-\infty < t < \infty$, $0 < \chi < \pi$, $0 < \theta < \pi$ and $0 \leq \phi < 2\pi$, with $\alpha = \sqrt{3/\Lambda}$. The term in brackets corresponds to the metric of a 3-sphere,

$$d\Omega_3^2 = d\chi^2 + \sin^2 \chi (d\theta^2 + \sin^2 \theta d\phi^2),$$

the set of points equidistant from a fixed point, embedded in a 4-dimensional Euclidean space. Intersections parallel to the equator of the 3-sphere (constant χ hypersurfaces) give 2-spheres of radius $\sin^2 \chi$. Since $0 < \chi < \pi$, both poles are actually points, 2-spheres of zero radius.

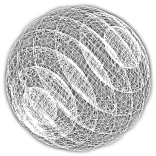

Figure 16: Projection of a 3-sphere S^3 into 3D space. Figure from Wikipedia.

In order to study the infinities at the de Sitter spacetime the following coordinate is chosen [10],

$$T = 2 \arctan[\exp(t/\alpha)] - \pi/2, \tag{6.2}$$

with $-\pi/2 < T < \pi/2$. The metric (6.1) transforms then into

$$ds^2 = \Xi(T) d\tilde{s}^2 = \alpha^2 \cosh^2(T/\alpha)[-dT^2 + d\Omega_3^2], \tag{6.3}$$

Note the similarity between equations (6.3) and (3.9). Both Minkowski and de Sitter spaces are conformal to the spacetime solution given in brackets, known as the Einstein static universe. The region conformal to the de Sitter space is thus given by

$$-\pi/2 < T < \pi/2, \qquad 0 < \chi < \pi. \tag{6.4}$$

The Penrose diagram of the de Sitter spacetime is therefore the following.

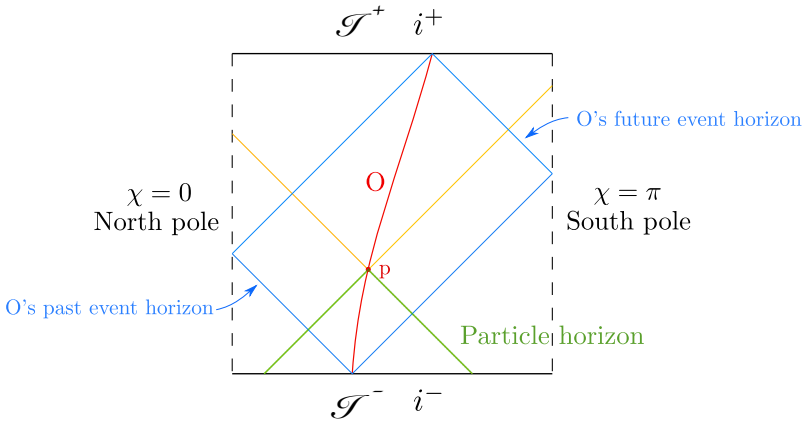

Figure 17: Penrose diagram for the de Sitter spacetime.

Note that both north and south poles are represented by timelike lines, in the same way as $r = 0$ at the Minkowski spacetime (see Figure 6). Besides, horizontal lines cutting the diagram represent 3-spheres, with the $\chi = 0$ and $\chi = \pi$ lines representing the north and south poles of the 3-sphere.

One of the main features of a de Sitter spacetime is that $\mathscr{I}^{\pm}$ are no longer drawn at $\pm 45^{\circ}$. Future and past null infinities are now spacelike hypersurfaces, and this leads to the existence of *particle* and *event horizons* for observers travelling at a de Sitter space. Consider an observer O with a trajectory like the one depicted in red in Figure 17. There can exist a number of timelike trajectories that begin at i^- which do not intersect with O's past light cone at p. Thus, particles following these trajectories have not been visible for O at p. The boundary of the region where particles that have been seen already lie is called *particle horizon*. Over time more events will be visible, and thus the particle horizon will increase in size.

On the other hand, there exists a *cosmological horizon* on O's world-line. The past null cone of O at $\mathscr{I}^+$ marks off a boundary between events that will and will not be visible. This boundary is the *future event horizon*. Moreover, the future null cone at $\mathscr{I}^-$ gives rise to the *past event horizon*. The cosmological horizons, namely the future event horizon together with the past event horizon, constitute the boundary for the events that observer O will never influence. In contrast with the Schwarzschild and Reissner-Nordström spacetimes, which have horizons defined relative to a fixed source, these horizons are observer dependent.

Besides, a particle crossing the future event horizon will be seen infinitely redshifted by observer O. Let us consider a second observer P with a trajectory like the one depicted in orange in Figure 18. In this case, such traveler will at some point cross O's future horizon at a finite time (say 4.0 seconds), while O takes infinite time to "arrive" at its own event horizon (it tends to $\mathscr{I}^+$, which is a boundary, it does never arrive there). Now, if P emits n periodic signals before crossing the EH, O will receive those n signals in an infinite time, and each signal will take every time more time to be observed by O. This is, observer O will watch P infinitely redshifted. Note this is an effect by virtue of the existence of an event horizon.

It must be stressed that the existence of all the mentioned horizons is exclusively due to the spacelike character of $\mathscr{I}^{\pm}$. In contrast with Minkowski space, an observer reaching i^+ cannot "see" the entire spacetime. The "observable" spacetime region is limited by the future event horizon.

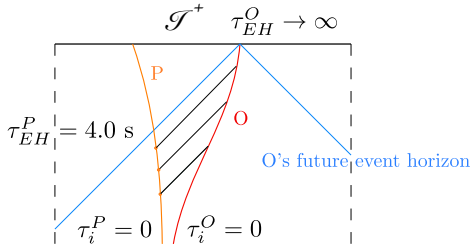

Figure 18: A schematic illustration of the redshift effect.

Finally, it is convenient to introduce the de Sitter metric in terms of the spherical coordinates $(t,\ r,\ \theta,\ \phi)$, since the displayed black hole solutions are written in this coordinate system. The metric is then given by

$$ds^2 = -\left(1 - \frac{\Lambda r^2}{3}\right) dt^2 + \left(1 - \frac{\Lambda r^2}{3}\right)^{-1} dr^2 + r^2 d\Omega^2, \tag{6.5}$$

with $-\infty < t < \infty$, $0 < r < \sqrt{3/\Lambda}$, $0 < \theta < \pi$ and $0 \leq \phi < 2\pi$, which only cover the region I of the following de Sitter conformal diagram, a quarter of the complete de Sitter spacetime. This is why the coordinates $(t,\ \chi,\ \theta,\ \phi)$ have been first introduced in this section. In the de Sitter space, the coordinates $(t,\ r,\ \theta,\ \phi)$ do not cover the entire spacetime manifold.

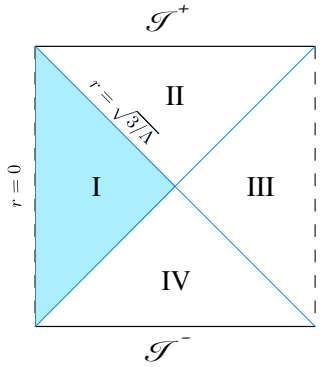

Figure 19: Conformal structure of the de Sitter solution.

The null hypersurfaces, which are at $r = \sqrt{3/\Lambda}$, are in fact the past and future event horizons of an observer at $r = 0$ (also $\chi = 0$ or $\chi = \pi$), at one of the poles of the 3-sphere. We will refer to these as the cosmological horizon of the de Sitter universe. Additionally, let us stress the similarity of the conformal structure of de Sitter with the Minkowski space.

6.2 The Schwarzschild - de Sitter solution

The simplest generalization of the de Sitter solution is the Schwarzschild-de Sitter (SdS) space, which represents a black hole inmersed in a universe with positive cosmological constant. Its metric is given by

$$ds^2 = -\Delta dt^2 + \Delta^{-1} dr^2 + r^2 d\Omega^2, \tag{6.6}$$

where

$$\Delta(r) = \left(1 - \frac{2m}{r} - \frac{\Lambda r^2}{3}\right), \tag{6.7}$$

which reduces to the Schwarzschild metric if $\Lambda = 0$, or to the de Sitter space if $m = 0$. If $0 < 9\Lambda m^2 < 1$ [8], the metric function (6.7) has two different positive real roots, which correspond to two horizons: $r = r_b$ a black hole event horizon and $r = r_c$ a de Sitter cosmological horizon, such that $r_c > r_b > 0$. The third root is negative and therefore does not have a physical meaning.

With two zeros, in the same way as in the Reissner-Nordström space, the Schwarzschild - de Sitter spacetime has three different regions depending on the covered interval of the coordinate r: regions I ($r_b < r < r_c$), II ($0 < r < r_b$) and III ($r_c < r < \infty$).

Once again, in order to obtain the maximal extension of the spacetime manifold, the Kruskal-Szekeres coordinates can be considered. Just as in the RN space, two patches are "combined", and overlap in region I. The coordinate compactification process that must be followed is analogous to the one explained already. Since these steps are similar to the ones showed, and since the aim of the work is to focus on Reissner-Nordström-de Sitter black holes, they will not be given in the present section. The global conformal structure is illustrated in Figure 20.

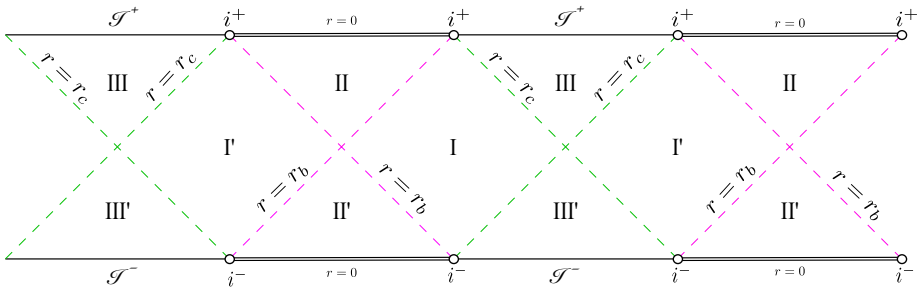

Figure 20: Part of the infinitely extendible Penrose diagram of the Schwarzschild - de Sitter spacetime when $0 < 9\Lambda m^2 < 1$.

First of all, it should be stressed that the SdS spacetime can be infinitely extended. The above diagram is just a small part of the whole of the periodic Penrose diagram. Thus, the extended conformal diagram would describe the causal structure of infinite Schwarzschild black holes living in infinite identical de Sitter universes. Mathematically, it may be natural to extend the conformal structure but, an observer in such spacetime would "see" a single black hole. A more "realistic" case might be the one depicted in Figure 21.

Such structure has some of the features of both the Schwarzschild and de Sitter solutions. The real physical singularity at $r = 0$, together with the event horizon dividing regions I and II reflect the presence of a Schwarzschild solution. On the other hand, the "effect" of the de Sitter background is reflected on the spacelike character of the future and null infinities $\mathscr{I}^{\pm}$ and the associated cosmological horizon at $r = r_c$. This is the "effect" of adding a positive cosmological constant to the Schwarzschild solution (compare Figures 20 and 9).

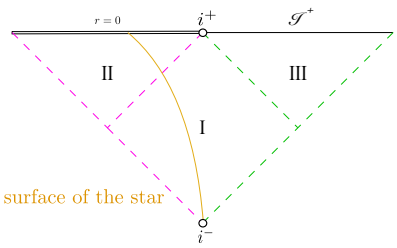

Figure 21: Penrose diagram of a single Schwarzschild black hole in a de Sitter spacetime.

7 Charged Black Holes with Cosmological Constant

While the maximal analytic extension of the Reissner-Nordström solution has been deeply studied, not many works can be found for charged black holes in a de Sitter background. Some shortly discuss certain aspects [12], [11], [6], and has been studied in the most complete and general case in [14]. In this section, a more explicit derivation follows in order to achieve a maximal analytical extension, together with the construction of the Penrose diagram.

7.1 The Reissner-Nordström-de Sitter solution

The Reissner-Nordström-de Sitter (RNdS) solution is the solution to Einstein's equation for a non-rotating charged black hole with positive cosmological constant. The RNdS solution is given by

$$ds^2 = -\Delta dt^2 + \Delta^{-1} dr^2 + r^2 d\Omega^2, \tag{7.1}$$

where

$$\Delta(r) = \left(1 - \frac{2m}{r} + \frac{e^2}{r^2} - \frac{\Lambda r^2}{3}\right). \tag{7.2}$$

The function Δ has one negative root at $r = r_0$, and either one or three positive roots. Special cases of double and triple roots can also occur as it is studied in [4]. In this work only the case with three positive roots will be analysed. As mentioned, positive roots are associated to specific horizons. The first two roots correspond to the two horizons of the Reissner-Nordström space, the event and Cauchy horizons at $r = r_+$ and $r = r_-$ respectively. The third one is the cosmological horizon at $r = r_c$ which is associated to the de Sitter solution. These three horizons, such that $r_- < r_+ < r_c$, "divide" the spacetime into four regions, the three regions of the RN space plus the one due to the spacelike behaviour of the future and null infinities at the de Sitter space:

- Region I: $r_+ < r < r_c$
- Region II: $r_- < r < r_+$
- Region III: $0 < r < r_-$
- Region IV: $r_c < r < \infty$

With four different regions, *three* Kruskal-Szekeres *patches* are needed to cover the RNdS spacetime manifold [14].

- Coordinates $\{u_c, v_c\}$ relate regions I and IV. For this region the metric (7.1) can be written as [14]

$$ds^2 = \frac{4a_c^2\ \Delta(r)}{\kappa_c(r)}\ du_c dv_c + r^2 d\Omega^2\ . \tag{7.3}$$

(The constant a_c and the function $\kappa_c(r)$ are defined below.)

- Coordinates $\{u_+, v_+\}$ relate regions I and II, just as in the RN space, in which the line element converts into

$$ds^2 = \frac{4a_+^2\ \Delta(r)}{\kappa_+(r)}\ du_+ dv_+ + r^2 d\Omega^2. \tag{7.4}$$

- Coordinates $\{u_-, v_-\}$ relate regions II and III (as in the RN solution as well). The metric in this region is given by,

$$ds^2 = \frac{4a_-^2\ \Delta(r)}{\kappa_-(r)} du_- dv_- + r^2 d\Omega^2. \tag{7.5}$$

Now, let us set the following notation: r_- as r_1, r_+ as r_2 and r_c as r_3, and recall we have a negative root ($r = r_0$). With this notation, the constant a_i and function $\kappa_i(r)$ displayed in equations (7.3), (7.4) and (7.5) are determined by the expressions [14]

$$a_i = -\frac{3r_i^2}{\Lambda} \prod_{j\neq i, j=0}^{3} \frac{1}{(r_i - r_j)}\ ,$$

and

$$\kappa_i(r) = (-1)^i e^{a/a_i}(r_i - r) \prod_{j\neq i, j=0}^{3} |r - r_j|^{a_j/a_i}\ ,$$

where,

$$a = -\sum_{i=0}^{3} a_i \ln|P_2 - r_i|\ ,\ \text{with}\ \ P_2 = \frac{3m + \sqrt{9m^2 - 8e^2}}{2}\ .$$

The relation between the Kruskal-Szekeres coordinates and the function r is given by the following expression [14],

$$r(u_*, v_*) = \frac{u_* v_*}{\kappa_*}, \tag{7.6}$$

where $\{u_*, v_*\}$ stands for each of the three pairs of coordinates $\{u_c, v_c\}$, $\{u_+, v_+\}$ and $\{u_-, v_-\}$.

Now, we need to combine these three charts considering that the $\{u_c, v_c\}$ patch covers regions I and IV ($r_+ < r < \infty$), the $\{u_+, v_+\}$ patch regions I and II ($r_- < r < r_c$), and the $\{u_-, v_-\}$ patch regions II and III ($0 < r < r_+$). These coordinates have infinite range and thus, the first step is to compactify these using the tangent function,

$$\tan U_* = u_*, \qquad \tan V_* = v_*.$$

The coordinate ranges are thus finite now, $-\pi/2 < U_* < \pi/2$, $-\pi/2 < V_* < \pi/2$. As mentioned, the next step consists on obtaining spacelike and timelike coordinates given by,

$$T_* = U_* + V_*, \qquad R_* = U_* - V_*,$$

which lead to

$$-\pi < T_* + R_* < \pi, \qquad -\pi < T_* - R_* < \pi, \tag{7.7}$$

Besides, there are two more range conditions that have to be accounted for. Since the coordinate r in equation (7.1) has the range $0 < r < \infty$, in particular $r > 0$, equation (7.6) yields,

$$u_- v_- < 1. \tag{7.8}$$

This condition only relates to the patch associated to region III, $\{u_-, v_-\}$. After the coordinate compactification, equation (7.8) transforms into $-\pi/2 < T_- < \pi/2$.

Regarding the second condition, as mentioned, at large distances the de Sitter spacetime becomes relevant, more than the black hole solution. In order to study the infinities at the Reissner-Nordström-de Sitter spacetime, it may be then reasonable to consider a similar compactification relation of the coordinate t applied at the de Sitter spacetime, equation (6.2),

$$T_c = 2\arctan[\exp(t/\gamma)] - \pi/2, \tag{7.9}$$

where γ is a non-zero constant that depends on the characteristic parameters of the RNdS space.

Thus, in addition to the conformal region given in (7.7), the $\{u_c, v_c\}$ patch has the following range condition: $-\pi/2 < T_c < \pi/2$.

So far, the conformal regions of the three charts have been determined, and have the following shape (see Figure 22).

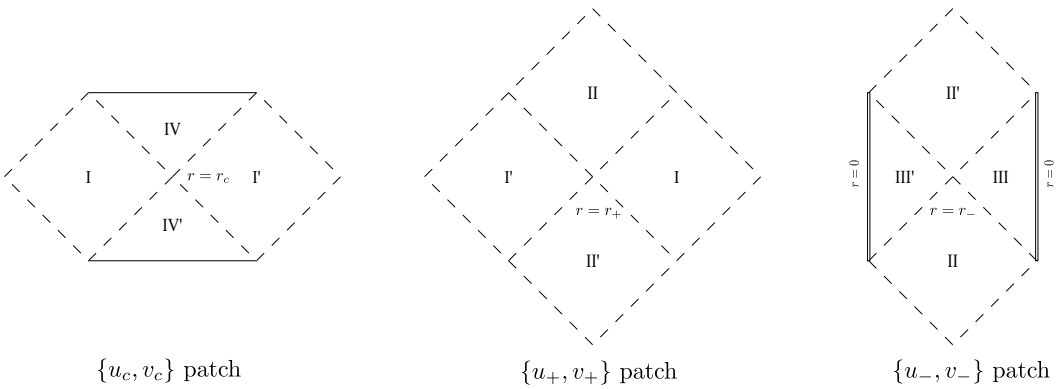

Figure 22: Illustration of the covered conformal region of the three patches that will form the global conformal structure of the Reissner-Nordström-de Sitter spacetime.

In the case of the $\{u_-, v_-\}$ patch, coordinate T_c is timelike, since, as it can be shown, constant t hypersurfaces are timelike in region II. Hence, the character of the singularity $r = 0$.

Eventually, after the compactifying process has been performed, we can combine the three patches and build the Penrose diagram of the present spacetime solution (see Figure 23).

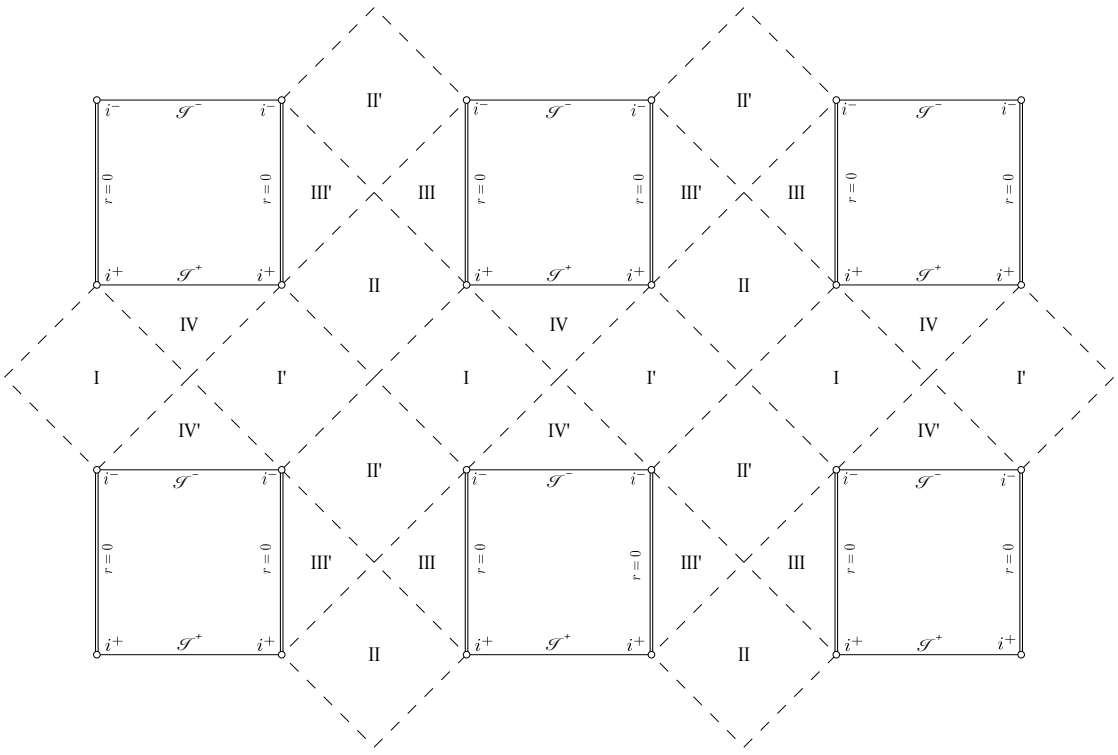

Figure 23: Penrose diagram of the Reissner-Nordström-de Sitter metric.

Let us first note that the spacetime diagram can be infinitely extended in both timelike and spacelike directions. In the same way as in the Reissner-Nordström spacetime, it might be natural to combine the three different patches indefinitely. The result is a grid with timelike and spacelike boundaries at $r = 0$ and $r \to \infty$, representing an infinite number of charged black holes in infinite de Sitter universes. Nevertheless, an observer in such spacetime living in a specific universe would only "see" one black hole, and thus, a more physically realistic case may be the one depicted in the following diagram.

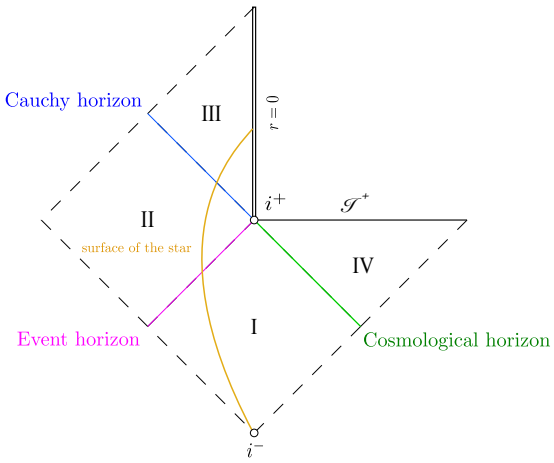

Figure 24: A more realistic Penrose diagram of the Reissner-Nordström-de Sitter metric.

In comparison with the Reissner-Nordström solution (see Figure 14), the above diagram clearly shows the effect of adding a positive cosmological constant to such black hole solution. The Reissner-Nordström-de Sitter spacetime is not an asymptotically flat solution, and as every de Sitter-like solution, no asymptotically flat end structure appears at the Penrose diagram. Besides, apart from the event and Cauchy horizons of the RN space, one more horizon appears at the spacetime: the cosmological horizon.

In the RN space, an observer about to cross the Cauchy horizon would first see the entire universe (light could arrive from the spatial infinity i^0), and after crossing such horizon (let us imagine for a moment that the Cauchy horizon is stable) it would only see the light coming from the region $0 < r < r_-$, where the singularity is. Suddenly, the universe would seem to "collapse". Having a de Sitter background would change completely the observer's view. This time, before crossing the Cauchy horizon, it would only see part of the universe, since the observable universe is limited by the cosmological horizon. The region IV, such that $r_c < r < \infty$, looks as if it was "hidden" from the observer. Thus, in the RNdS spacetime, the universe would appear to "collapse" in a less "violent" way.

Besides, the Cauchy horizon of the Reissner-Nordström-de Sitter solution appears to be stable under certain circumstances. For example, when the surface gravity (κ) at the cosmological horizon is higher than at the Cauchy horizon [6], or for charged scalar perturbations with angular momentum $l \geq 1$ [19]. These results are in apparent contradiction with the strong cosmic censorship proposed by Penrose, and could also reveal the effect of having a positive cosmological constant (recall the Reissner-Nordström space was unstable). Despite the important efforts, there is still no mathematical demonstration that proves the stability of the Reissner-Nordström-de Sitter solution.

8 Conclusions

Penrose diagrams are a powerful tool to study the causal structure of a spherically symmetric spacetime solution in General Relativity. The study of causal relationships in a spacetime manifold is equivalent to that of the conformally related geometry. Thus, a conformally compactified spacetime where infinity is located a finite value away will make this structure much more evident. In general, this compactification process "divides" infinity into five different "regions": $i^{\pm}$, i^0 and $\mathscr{I}^{\pm}$, the future and past timelike infinities, the spacelike infinity and the future and past null infinities, respectively. Besides, null geodesics can help determine different type of horizons. These ideas have been reflected in the Minkowski, Schwarzschild, Reissner-Nordström (RN) and de Sitter solutions, which were convenient to introduce in order to understand the Reissner-Nordström-de Sitter solution.

With the construction of the Penrose diagram, we have learned that the Reissner-Nordström solution has two types of horizons: an event horizon (as in the Schwarzschild black hole) and a Cauchy horizon. An event horizon is defined as the distance at which light cannot escape due to the gravitational pull of the black hole and therefore, geodesics inside the event horizon will not reach the future null infinity $\mathscr{I}^+$. Besides, a Cauchy horizon is a boundary of the domain of validity of an initial value problem. On the other hand, a de Sitter spacetime solution has a cosmological horizon due to the spacelike character of the future and past null infinities $\mathscr{I}^{\pm}$. Moreover, while Minkowski, Schwarzschild, and Reissner-Nordström spacetimes are asymptotically flat solutions, de Sitter-like spacetime solutions are not, as it has been reflected in both de Sitter and de Sitter-Schwarzschild (SdS) solutions. This property is displayed on the appearance of an asymptotically flat end structure at the Penrose diagrams of the former solutions.

Eventually, we have completed a study of a charged black hole with positive cosmological constant, which is given by the Reissner-Nordström-de Sitter metric. This solution has three types of horizons: an event, Cauchy and cosmological horizon. This is highly reasonable, considering that the solution is given by a composition of both RN and de Sitter solutions. In the same way as in the RN and SdS spacetimes, the conformal diagram can be infinitely extended, and in this case, spacelike and timelike boundaries appear at $r \to \infty$ and $r = 0$. Nevertheless, the extended Penrose diagram is probably not realistic, and a more physically relevant diagram has been proposed.

Along the way, we have found interesting aspects that in the end have not been studied. The study of the nature of both future and past timelike infinities, the vision one would have when crossing the Cauchy horizon at both, Reissner-Nordström and Reissner-Nordström-de Sitter spacetimes, or the study of instabilities at these last solutions are some of the ideas that are left open for the future.

To conclude, let us note, again, the importance of Penrose diagrams for the study of causality of spherically symmetric spacetime solutions. In the end, causality is fundamental to any physical model that describes nature.

References

[1] B. P. Abbott, R. Abbott, T. Abbott, M. Abernathy, F. Acernese, K. Ackley, C. Adams, T. Adams, P. Addesso, R. Adhikari et al. (2016) *Observation of gravitational waves from a binary black hole merger.* Physical review letters **116** 061102.

[2] R. Abuter, A. Amorim, N. Anugu, M. Bauböck, M. Benisty, J. Berger, N. Blind, H. Bonnet, W. Brandner, A. Buron et al. (2018) *Detection of the gravitational redshift in the orbit of the star S2 near the Galactic centre massive black hole.* Astronomy & Astrophysics **615** L15.

[3] A. Alberdi, J. Gómez Fernández, E. H. T. Collaboration et al. (2019) *First M87 Event Horizon Telescope Results. I. The Shadow of the Supermassive Black Hole* .

[4] D. R. Brill and S. A. Hayward (1994) *Global structure of a black hole cosmos and its extremes.* Classical and Quantum Gravity **11** 359.

[5] S. M. Carroll, *Spacetime and geometry. An introduction to general relativity* (2004).

[6] C. M. Chambers (1997) *The Cauchy horizon in black hole-de Sitter spacetimes.* arXiv preprint gr-qc/9709025 .

[7] S. Chandrasekhar and J. B. Hartle (1982) *On crossing the Cauchy horizon of a Reissner–Nordström black-hole.* Proceedings of the Royal Society of London. A. Mathematical and Physical Sciences **384** 301–315.

[8] J. B. Griffiths and J. Podolskỳ, *Exact space-times in Einstein's general relativity* (Cambridge University Press 2009).

[9] S. Hawking and R. Penrose, *The nature of space and time* (Princeton University Press 2010).

[10] S. W. Hawking and G. F. R. Ellis, *The large scale structure of space-time*, vol. 1 (Cambridge university press 1973).

[11] K. Lake (1979) *Reissner-Nordström-de Sitter metric, the third law, and cosmic censorship.* Physical Review D **19** 421.

[12] H. Laue and M. Weiss (1977) *Maximally extended Reissner-Nordström manifold with cosmological constant.* Physical Review D **16** 3376.

[13] C. W. Misner, K. S. Thorne, J. A. Wheeler and D. I. Kaiser, *Gravitation* (Princeton University Press 2017).

[14] M. Mokdad (2017) *Reissner–Nordstrøm–de Sitter manifold: photon sphere and maximal analytic extension.* Classical and Quantum Gravity **34** 175014.

[15] R. Penrose (2011) *Republication of: Conformal treatment of infinity.* General Relativity and Gravitation **43** 901–922.

[16] M. Simpson and R. Penrose (1973) *Internal instability in a Reissner-Nordström black hole.* International Journal of Theoretical Physics **7** 183–197.

[17] P. K. Townsend (1997) *Lecture notes for a 'Part III' course 'Black Holes' given in DAMTP, Cambridge.* arXiv preprint gr-qc/9707012 .

[18] R. M. Wald, *General relativity* (University of Chicago Press (Chicago, 1984) 2007).

[19] Z. Zhu, S.-J. Zhang, C. Pellicer, B. Wang and E. Abdalla (2014) *Stability of Reissner-Nordström black hole in de Sitter background under charged scalar perturbation.* Physical Review D **90** 044042.